INORGANIC CHEMISTRY
FRONTIERS

RESEARCH ARTICLE

View Article Online
View Journal | View Issue

Cite this: *Inorg. Chem. Front.*, 2022, **9**, 5820

Interesting dimensional transition through changing cations as the trigger in multinary thioarsenates displaying variable photocurrent response and optical anisotropy†

Chao Zhang,[a] Sheng-Hua Zhou,[b,c,d] Yu Xiao,[a] Hua Lin *[b,c,d] and Yi Liu *[a]

Received 4th August 2022,
Accepted 19th September 2022

DOI: 10.1039/d2qi01694j

rsc.li/frontiers-inorganic

Due to the intriguing component variability and structure–property flexibility, lone-pair cation-based chalcogenides have garnered substantial interest in recent years. Herein, two new multinary thioarsenates, $Cs_2ZnAs_4S_8$ and $[(NH_4)Cs]CdAs_4S_8$, were successfully discovered *via* a surfactant–thermal reaction. Both of them possess identical stoichiometry 2–1–4–8, but they exhibit surprisingly different structural features. $Cs_2ZnAs_4S_8$ demonstrates a three-dimensional (3D) $[ZnAs_4S_8]^{2-}$ framework made from the corner-sharing $[ZnS_4]$ tetrahedra and one-dimensional (1D) $[As_4S_8]^{4-}$ chains, whereas $[(NH_4)Cs]CdAs_4S_8$ exhibits a two-dimensional (2D) $[CdAs_4S_8]^{2-}$ layer constructed from the corner-sharing $[CdS_4]$ tetrahedra and tetranuclear $[As_4S_8]$ clusters. Photoelectric measurements display that $Cs_2ZnAs_4S_8$ has higher photogenerated electron–hole pair separation efficiency than $[(NH_4)Cs]CdAs_4S_8$ under visible light irradiation. Moreover, both of them show large optical anisotropy (Δn > 0.17 at 1064 and 2050 nm), while the low dimensional structure is more conducive to enhancing the optical anisotropy based on the theoretical calculations. These findings will provide inspiration for the exploration of multifunctional chalcogenides.

Introduction

Over the past few decades, inorganic chalcogenides containing $[M^{III}Q_n]$ (M^{III} = As, Sb, Bi) polyhedra have attracted increasing attention because of their intriguing structural and compositional diversity.[1–15] These M^{III} cations with stereochemically active lone-pair electrons are favorable to form different asymmetric coordination modes, which will further influence the electronic structures and physical properties of the resultant chalcogenides. For example, $M_2As_2Q_5$ (M = Ba, Pb; Q = S, Se) exhibit excellent overall infrared nonlinear optical (IR-NLO) performance thanks to their zero-dimensional (0D) discrete arsenate anions.[12] Pentanary thioantimonate $Rb_2Ba_3Cu_2Sb_2S_{10}$ adopts a one-dimensional (1D) chain structure and displays a wide-bandgap and an intriguing photocurrent response.[9] The narrow gap semiconductor $RbBi_{11/3}Te_6$, which consists of a two-dimensional (2D) infinite Bi_2Te_3-like layer, exhibits a sharp superconducting transition at ~3.2 K.[4] The three-dimensional (3D) frameworks $A_3Mn_2Sb_3S_8$ (A = K and Rb) not only display IR-NLO performances but also possess temperature-dependent paramagnetism and photocurrent responses.[13] On the other hand, transition-metal-based chalcogenides with d^{10} electronic configurations (*e.g.*, Zn^{2+}, Cd^{2+}, Hg^{2+}) have also been extensively investigated as these cations tend to show flexible coordination geometries, and hence engender an efficient route to design functional materials.[16] For instance, $Na_6Zn_3M_2Q_9$ (M = Ga, In; Q = S, Se), 2D layered chalcogenides made of unprecedented T_3-supertetrahedra, exhibit desirable photoluminescence performances.[17] $KCd_3Ga_5S_{11}$ adopts a diamond-like framework structure and achieves a strong second-harmonic-generation intensity (1.7 × $AgGaS_2$).[18] Ternary IR-NLO $BaHgSe_2$ shows large susceptibility and physicochemical stability activated by the trigonal planar $[HgSe_3]^{4-}$ motif.[19]

A tremendous amount of multinary lone-pair cation-based chalcogenides have been discovered so far, however, the systematic investigation of the A/TM/As/Q system (A = alkali metals; TM = group 12 metals; Q = chalcogen) is rarely reported. To the best of our knowledge, only 3 compounds in this system are known, namely $NaCdAsS_3$,[20] $Rb_4CdAs_2S_9$,[21] and

[a]*Institute for Composites Science Innovation (InCSI), School of Materials Science and Engineering, Zhejiang University, Hangzhou 310027, China.*
E-mail: liuyimse@zju.edu.cn
[b]*State Key Laboratory of Structural Chemistry, Fujian Institute of Research on the Structure of Matter, Chinese Academy of Sciences, Fuzhou, Fujian 350002, China.*
E-mail: linhua@fjirsm.ac.cn
[c]*Fujian Science & Technology Innovation Laboratory for Optoelectronic Information of China, Fuzhou, Fujian 350108, China*
[d]*University of Chinese Academy of Sciences, Beijing 100049, China*

†Electronic supplementary information (ESI) available: Additional experimental and theory results, together with additional tables and figures. CCDC 2167064 and 2167065. For ESI and crystallographic data in CIF or other electronic format see DOI: https://doi.org/10.1039/d2qi01694j

$CsHgAsS_3$.[22] The first two are obtained by the solid-state method, while the last one is prepared by solvothermal synthesis. Recently, a surfactant–thermal reaction has been proved to be a facile method for exploring novel chalcogenides.[23–31] In this study, our continuous explorations based on the surfactant–thermal method have led to the discovery of two new thioarsenates, $Cs_2ZnAs_4S_8$ and $[(NH_4)Cs]CdAs_4S_8$. Although these two compounds have identical stoichiometry 2–1–4–8, they are not isostructural and undergo an interesting dimensional transition from a 3D framework to a 2D layered structure. Herein, the crystal structure, physical properties, and corresponding theoretical studies are systematically investigated.

Results and discussion

Single-crystal X-ray diffraction (SXRD) test results show that $Cs_2ZnAs_4S_8$ and $[(NH_4)Cs]CdAs_4S_8$ belong to different space groups, *i.e.*, tetragonal $I4_1/a$ (no. 88) for $Cs_2ZnAs_4S_8$ with cell parameters of $a = b = 11.0828(5)$, $c = 13.2303(8)$ Å, and $Z = 4$ and tetragonal $P4/n$ (no. 85) for $[(NH_4)Cs]CdAs_4S_8$ with cell parameters of $a = b = 10.3879(2)$, $c = 7.7691(2)$ Å, and $Z = 2$. The detailed crystallographic information is listed in Table 1. There are 1 unique Cs atom (Wyckoff site: 8*e*), 1 unique As atom (Wyckoff site: 16*f*), 1 unique Zn atom (Wyckoff site: 4*a*), and 2 unique S atoms (Wyckoff sites: 16*f* and 16*f)* in its asymmetric unit (Table 2). As illustrated in Fig. 1a, the three-dimensional (3D) crystal structure of $Cs_2ZnAs_4S_8$ is constructed from charge-balanced Cs^+ cations, regular $[ZnS_4]$ tetrahedra, (Fig. 1b) and one-dimensional (1D) anionic chains $[As_4S_8]^{4-}$ made of the corner-sharing $[As_4S_9]$ groups (Fig. 1c). The important bond distances of $Cs_2ZnAs_4S_8$ are listed in Table S1.† The As atom adopts a common coordination with 3 S atoms in the bond distance range of 2.2143(5)–2.3267(5) Å to build a $[AsS_3]^{3-}$ triangular pyramid. The Zn–S bond distance in the $[ZnS_4]$ tetrahedron is 2.3309(5) Å. The S–As–S angles in $Cs_2ZnAs_4S_8$ range from 98.07(2)° to 103.28(2)°, while the S–Zn–S angles vary from 105.79(2)° to 117.12(2)°. These bond distances and angles in $Cs_2ZnAs_4S_8$ are normal and can also be comparable to the reported Cs-based chalcogenides.[32–34]

There are 7 unique crystallographic atoms in the asymmetric unit of the structure of $[(NH_4)Cs]CdAs_4S_8$, including 1 Cs (Wyckoff site: 2*c*), 1 Cd (Wyckoff site: 2*a*), 1 As (Wyckoff site: 8*g*), 2 S (Wyckoff sites: 8*g* and 8*g*), 1 N (Wyckoff site: 2*b*) and 1 H (Wyckoff site: 8*g*) (Tables 1 and 2). As given in Fig. 1d, the crystal structure of $[(NH_4)Cs]CdAs_4S_8$ is composed of regular $[CdS_4]$ tetrahedra with $d_{(Cd-S)} = 2.5481(5)$ Å and tetranuclear $[As_4S_8]$ clusters with $d_{(As-S)} = 2.2676(5)$–$2.3008(5)$ Å, which interconnect with each other by sharing vertexes to form a two-dimensional (2D) $[CdAs_4S_8]^{2-}$ layer filling the dispersed $(NH_4)^+$ and Cs^+ cations.

The interesting structural evolution between $Cs_2ZnAs_4S_8$ and $[(NH_4)Cs]CdAs_4S_8$ is illustrated in Fig. 1. Both of them possess an identical stoichiometry of 2–1–4–8 and belong to the same tetragonal system, but they are not isostructural and have some significantly different structural features: (i) pyramidal $[AsS_3]$ units in $Cs_2ZnAs_4S_8$ forms a 1D infinite $[As_4S_8]^{4-}$

Table 1 Crystallographic data and refinement details of $Cs_2ZnAs_4S_8$ and $[(NH_4)Cs]CdAs_4S_8$

Formula	$Cs_2ZnAs_4S_8$	$[(NH_4)Cs]CdAs_4S_8$
FW	887.35	819.51
Crystal system	Tetragonal	Tetragonal
Temperature (K)	Yellow	Orange
Crystal color	$I4_1/a$ (no. 88)	$P4/n$ (no. 85)
Space group	11.0828(5)	10.3879(2)
a (Å)	11.0828(5)	10.3879(2)
b (Å)	13.2303(8)	7.7691(2)
c (Å)	90	90
α (°)	90	90
β (°)	90	90
γ (°)	1625.06(18)	838.35(4)
V (Å^3)	4	2
Z	3.627	3.246
D_c (g cm^{-3})	15.004	12.243
μ (mm^{-1})	1.039	1.071
GOOF on F^2	0.0265, 0.0603	0.0152, 0.0300
R_1, wR_2 ($I > 2\sigma(I)$)[a]	0.0369, 0.0645	0.0189, 0.0316
R_1, wR_2 (all data)	1.826/−1.271	0.818/−0.552
Largest diff. peak/hole (e Å^{-3})	887.35	819.51

[a] $R_1 = \sum||F_o| - |F_c||/\sum|F_o|$, $wR_2 = [\sum w(F_o^2 - F_c^2)^2/\sum w(F_o^2)^2]^{1/2}$.

Table 2 Atomic coordinates and equivalent isotropic displacement parameters of $Cs_2ZnAs_4S_8$ and $[(NH_4)Cs]CdAs_4S_8$

Atom	Wyckoff	x	y	z	$U_{(eq)}$[a]	Occu.
$Cs_2ZnAs_4S_8$						
Cs	8*e*	0	0.25	0.45521(2)	0.02597(6)	1.0
As	16*f*	0.16243(2)	0.01798(2)	0.00487(2)	0.01245(5)	1.0
Zn	4*a*	0	0.25	0.125	0.01320(8)	1.0
S2	16*f*	0.17589(5)	0.21445(4)	0.03310(3)	0.01605(9)	1.0
S1	16*f*	0.31599(5)	0.51563(5)	0.10909(3)	0.01892(10)	1.0
$[(NH_4)Cs]CdAs_4S_8$						
Cs	2*c*	0.25	0.25	0.68028(3)	0.02210(7)	1.0
Cd	2*a*	0.25	0.75	0	0.01361(7)	1.0
As	8*g*	0.04860(2)	0.15875(2)	0.14479(2)	0.01204(6)	1.0
S2	8*g*	0.16315(4)	0.02562(4)	0.31813(6)	0.01556(10)	1.0
S1	8*g*	0.07233(4)	0.64420(4)	0.17643(6)	0.01402(9)	1.0
N	2*b*	0.25	0.75	0.5	0.0082(5)	1.0
H	8*g*	0.2013(19)	0.724(2)	0.446(3)	0.014(6)	1.0

[a] $U_{(eq)}$ is defined as one-third of the trace of the orthogonalized U_{ij} tensor.

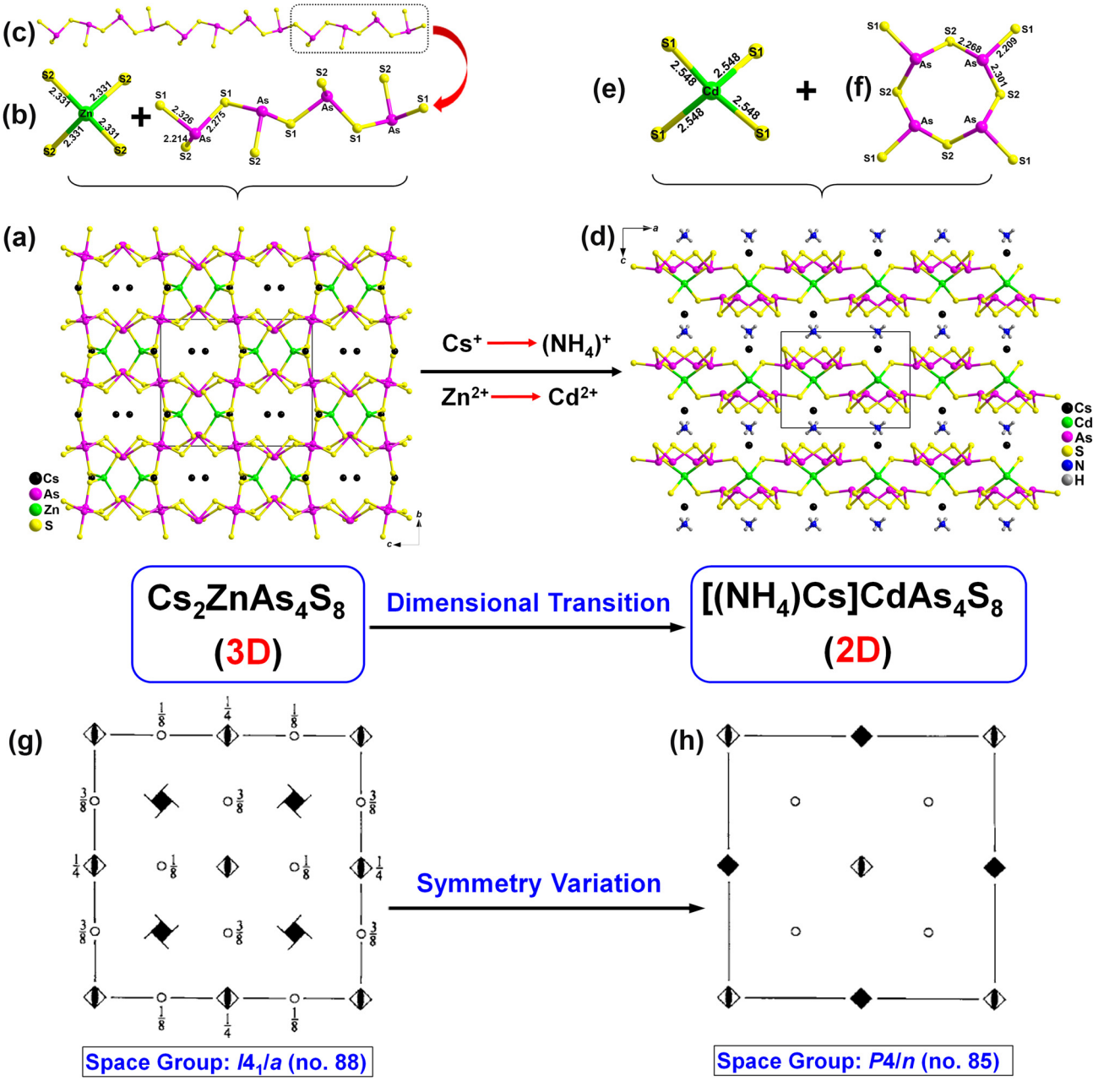

Fig. 1 Dimensional transition from 3D $Cs_2ZnAs_4S_8$ to 2D $[(NH_4)Cs]CdAs_4S_8$ based on the isovalent cation substitution. (a) Crystal structure of 3D $Cs_2ZnAs_4S_8$ viewed down the *a*-direction; (b) 1D $[As_4S_8]$ chain with the coordination environment of the $[As_4S_9]$ unit marked; (c) the coordination environment of the tetrahedral $[ZnS_4]$ unit; (d) crystal structure of 2D $[(NH_4)Cs]CdAs_4S_8$ viewed down the *a*-direction; (e, f) the coordination environment of the tetrahedral $[ZnS_4]$ unit and tetra-nuclear $[As_4S_8]$ cluster; (g, h) spatial symmetry operation from $I4_1/a$ (no. 88) to $P4/n$ (no. 85).

chain by vertex-sharing S1 atoms, while in $[(NH_4)Cs]CdAs_4S_8$, the tetra-nuclear $[As_4S_8]$ cluster is constructed from the same $[AsS_3]$ units; (ii) the coordination number (CN) of the crystallographically independent Cs atom in $Cs_2ZnAs_4S_8$ is 10 and the Cs–S bond distances are in the range of 3.617 (5)–4.116 (6) Å, which are different from those of $[(NH_4)Cs]CdAs_4S_8$ [CN = 8, $d_{(Cs-S)}$ = 3.696(5)–3.76(5) Å] (Fig. S1†). Such differences between them can be attributed to the different sizes of cations, *i.e.*, the 3D $[ZnAs_4S_8]^{2-}$ framework in $Cs_2ZnAs_4S_8$ can be viewed as $[ZnS_4]$ tetrahedra connected by 1D infinite $[As_4S_8]^{4-}$ chains by sharing S atoms and relatively large Cs^+ cations occupied the space of the framework. However, when one of the "large" radius Cs^+ cations was replaced by smaller radius $(NH_4)^+$ cations, the linkages between the $[As_4S_8]^{4-}$ chains in $Cs_2ZnAs_4S_8$ are broken, and the 3D $[ZnAs_4S_8]^{2-}$ framework in $Cs_2ZnAs_4S_8$ transforms into the 0D $[As_4S_8]$ clusters in $[(NH_4)Cs]CdAs_4S_8$. In addition, the above-mentioned structural evolution is ultimately reflected by their space groups, from $I4_1/a$ (for $Cs_2ZnAs_4S_8$) to $P4/n$ (for $[(NH_4)Cs]CdAs_4S_8$). The detailed symmetric operation change based on isovalent cation substitution is shown in Fig. 1g and h.

Polycrystalline samples of $Cs_2ZnAs_4S_8$ and $[(NH_4)Cs]CdAs_4S_8$ were prepared by a facile surfactant–thermal method at 413 K for 7 days with $CsOH{\cdot}H_2O$, Zn (or Cd), As_2S_3, S, oleic acid, hydrazine monohydrate (98%) and PEG-400 as staring materials, in a yield of approximately 80–90% based on Zn (or Cd) (further experimental details see the ESI†). As displayed in Fig. S2 and S3,† semi-quantitative energy-dispersive X-ray (EDX) elemental analysis provides the average atomic ratios of 2.0/1.1(2)/3.9(8)/8.2(1) and 1.0/1.1(4)/4.0(5)/7.9(7) for $Cs_2ZnAs_4S_8$ and $[(NH_4)Cs]CdAs_4S_8$, respectively. In addition, the purity of the polycrystalline samples was confirmed by powder X-ray diffraction (XRD) analysis (Fig. S4 and S5†). Moreover, both of them exhibit desirable thermal stability (up to 700 K) under N_2 conditions, as shown in Fig. S6 and S7.† Based on the different calculated formulas for direct semiconductors ($(\alpha h\nu)^2$ *vs.* energy) or indirect semiconductors ($(\alpha h\nu)^{1/2}$ *vs.* energy),[35] the experimental energy gaps (E_g) of $Cs_2ZnAs_4S_8$ and $[(NH_4)Cs]CdAs_4S_8$ are about 2.24 and 2.36 eV, respectively (Fig. 2). These values are compared to those of other reported quaternary thioarsenates, such as $RbCu_4AsS_4$ (E_g = 2.15 eV),[36] $Cs_3CuAs_4S_8$ (E_g = 2.26 eV),[30] $Rb_8Cu_6As_8S_{19}$ (E_g = 2.29 eV),[37] and $CsCu_2AsS_3$ (E_g = 2.30 eV).[27]

In addition, inspired by recent reports that most of the lone-pair-based chalcogenides display intriguing photocatalytic properties,[38–43] the photoelectrochemical experiment was performed through a standard three-electrode system using simulated solar light illumination to study the photoelectric properties of $Cs_2ZnAs_4S_8$ and $[(NH_4)Cs]CdAs_4S_8$. As illustrated in Fig. 3, the photocurrent–time curves exhibit a rapid and consistent photocurrent response in a multiple 20 s switching period. Clearly, $Cs_2ZnAs_4S_8$ shows a remarkable transient photocurrent response, which is about 4 times that of $[(NH_4)Cs]CdAs_4S_8$, that is, $Cs_2ZnAs_4S_8$ possesses higher photogenerated electron–hole pair separation efficiency than $[(NH_4)Cs]CdAs_4S_8$ under visible light irradiation. Meanwhile, these repeatable anodic photocurrent responses suggest that $Cs_2ZnAs_4S_8$ and $[(NH_4)Cs]CdAs_4S_8$ belong to n-type semiconductors. It is worth mentioning that these values of photocurrent densities (*ca.* 3.0 and 0.75 μA cm^{-2} for $Cs_2ZnAs_4S_8$ and $[(NH_4)Cs]CdAs_4S_8$, respectively) are much higher than those of most recently reported chalcogenides, such as $Rb_2Ba_3Cu_2Sb_2S_{10}$ (*ca.* 6 nA cm^{-2}),[9] BaCuSbSe$_3$ (*ca.* 30 nA cm^{-2}),[38] and BaCuSbS$_3$ (*ca.* 55 nA cm^{-2}).[38]

To well understand the origin of difference of electronic structures and structure–activity relationships, theoretical calculations of $Cs_2ZnAs_4S_8$ and $[(NH_4)Cs]CdAs_4S_8$ have been systematically carried out based on DFT methods. As shown in Fig. 4a and b, the valence band maximum (VBM) and the conduction band minimum (CBM) located at the same high-symmetry points (*i.e.*, Z|R) indicate that $Cs_2ZnAs_4S_8$ is a direct-band-gap (E_g = 1.92 eV) semiconductor, while $[(NH_4)Cs]CdAs_4S_8$ is an indirect-band-gap (E_g = 2.13 eV) semiconductor since the VBM and the CBM are located at different high-symmetry points (*i.e.*, Z|R and V, respectively). These calculated values are slightly smaller than the experimental observations

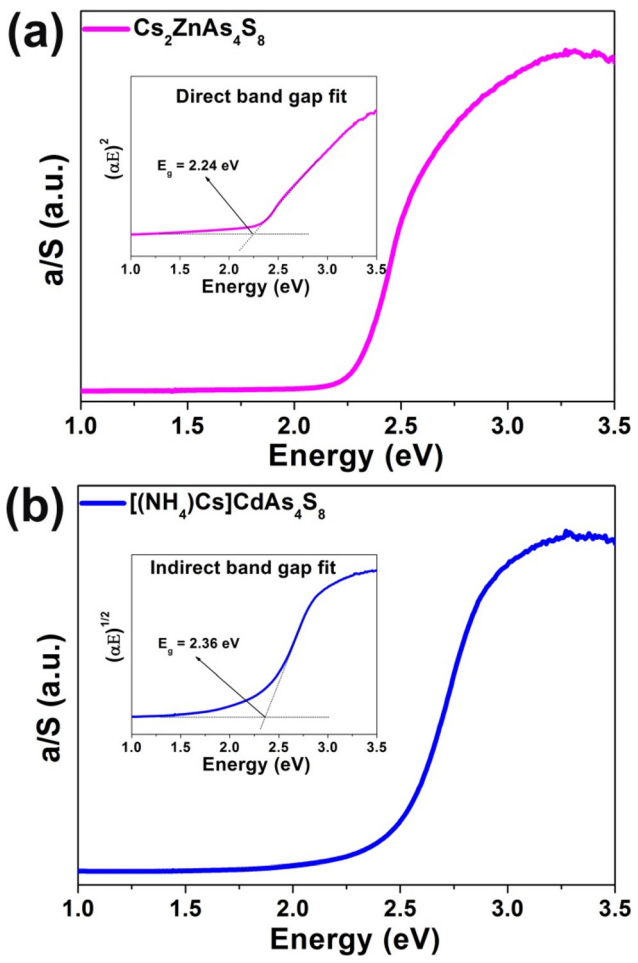

Fig. 2 UV-vis-NIR diffuse reflectance spectra of (a) $Cs_2ZnAs_4S_8$ and (b) $[(NH_4)Cs]CdAs_4S_8$ (inset: direct or indirect band gap fit based on the DFT results).

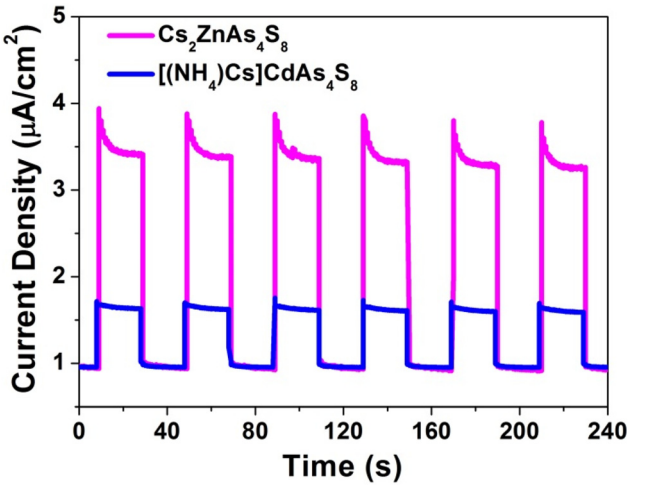

Fig. 3 Photocurrent response curves of $Cs_2ZnAs_4S_8$ and $[(NH_4)Cs]CdAs_4S_8$.

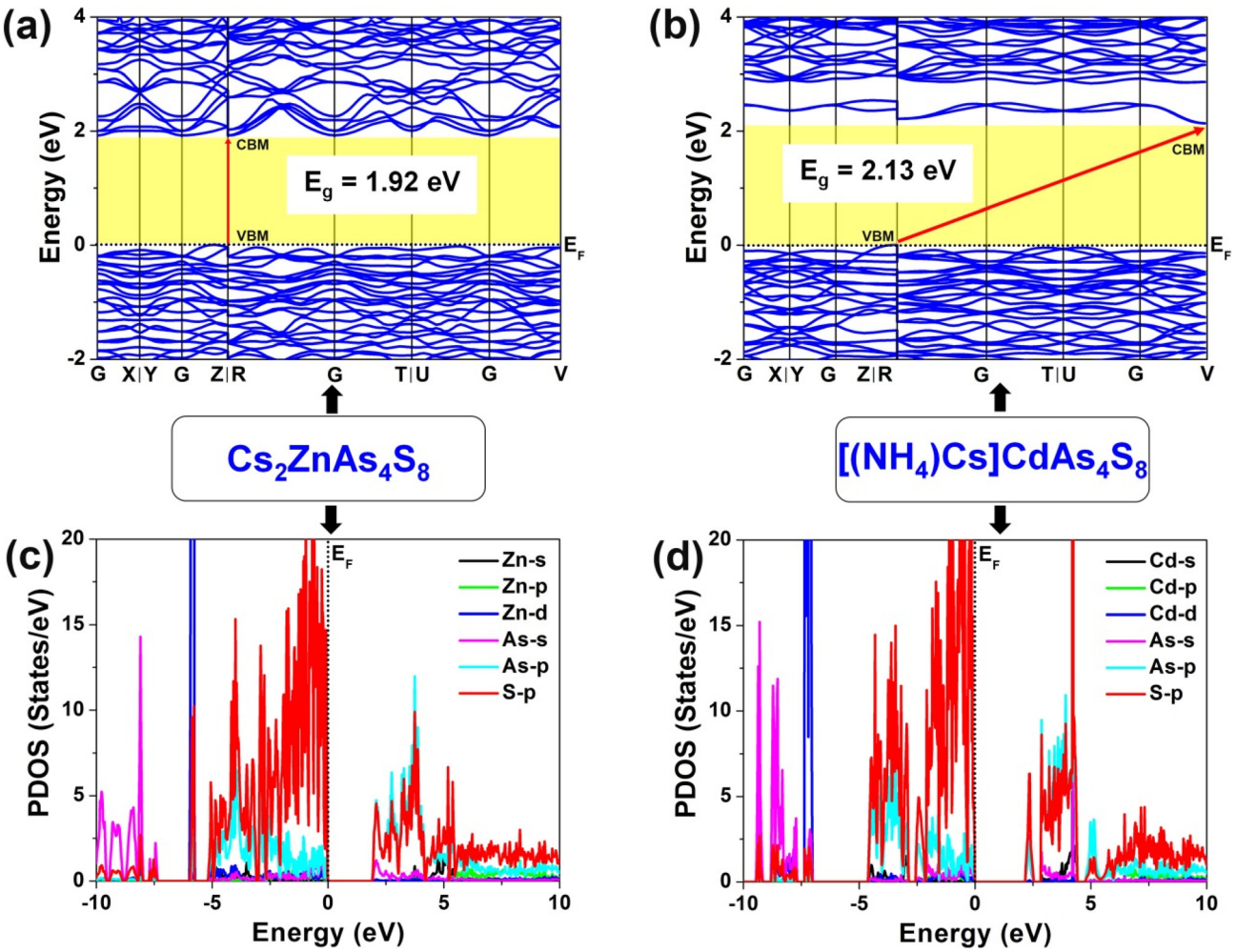

Fig. 4 Theoretical calculated results of $Cs_2ZnAs_4S_8$ and $[(NH_4)Cs]CdAs_4S_8$: (a, b) electronic band structures; (c, d) PDOSs ((states with fewer contributions are omitted for a better view). The Fermi level E_F is set at 0.0 eV.

(2.24 eV for $Cs_2ZnAs_4S_8$ and 2.36 eV for $[(NH_4)Cs]CdAs_4S_8$, as given in Fig. 2), which is a well-known phenomenon for the local approximations to DFT.[44] It is widely known that the photocatalytic activity mainly depends on the separation and diffusion rate of the photogenerated charge carriers, which can be judged by calculating the relative effective masses of electrons and holes based upon the electronic structures of the VBM and CBM in the title compounds.[38] Through comparison, we can clearly see that the electronic bands of $Cs_2ZnAs_4S_8$ are steeper than those of $[(NH_4)Cs]CdAs_4S_8$. Namely, $Cs_2ZnAs_4S_8$ is more conducive to improving the efficiency of photocatalysis, which is basically consistent with the experimental observation (Fig. 3). In addition, the projected density of states (PDOSs) with major contributions of title compounds is illustrated in Fig. 4c and d. $Cs_2ZnAs_4S_8$ and $[(NH_4)Cs]CdAs_4S_8$ exhibit similar results: the band from −5 eV to the Fermi level (EF), S-3p as well as As-4p and Zn-3d (or Cd-4d) states makes the main contribution, while the bottom of the CB is mainly composed of electronic hybridization of S-3p, As-4p and As-4s states. Consequently, the optical E_g values of $Cs_2ZnAs_4S_8$ and $[(NH_4)Cs]CdAs_4S_8$ mainly come from the charge transfer of Zn (or Cd)–S and As–S units, in which charge-balancing cations (*e.g.*, Cs^+, $(NH_4)^+$) show negligible contributions for the DOS. On the basis of their electron structures, we also calculated the birefringence (Δn) of $Cs_2ZnAs_4S_8$ and $[(NH_4)Cs]CdAs_4S_8$, respectively. As displayed in Fig. 5, their Δn values in both the important wavelengths can be calculated as 0.17@1064 nm and 0.18@2050 nm for $Cs_2ZnAs_4S_8$ and 0.29@1064 nm and 0.31@2050 nm for $[(NH_4)Cs]CdAs_4S_8$, which are comparable with some recently reported chalcogenides, indicating that they have potential as UV-vis or IR birefringent crystals. As known, the Δn value will mainly depend on the anisotropy of the anionic substructure, whereas the contribution of charge-balancing cations can be neglected.[45–50] In other words, compared with the 3D anionic $[CdAs_4S_8]^{2-}$ framework in $[(NH_4)Cs]CdAs_4S_8$, the anisotropy of the 2D anionic $[ZnAs_4S_8]^{2-}$ layer in $Cs_2ZnAs_4S_8$ is more obvious, which is more beneficial for producing larger Δn values.

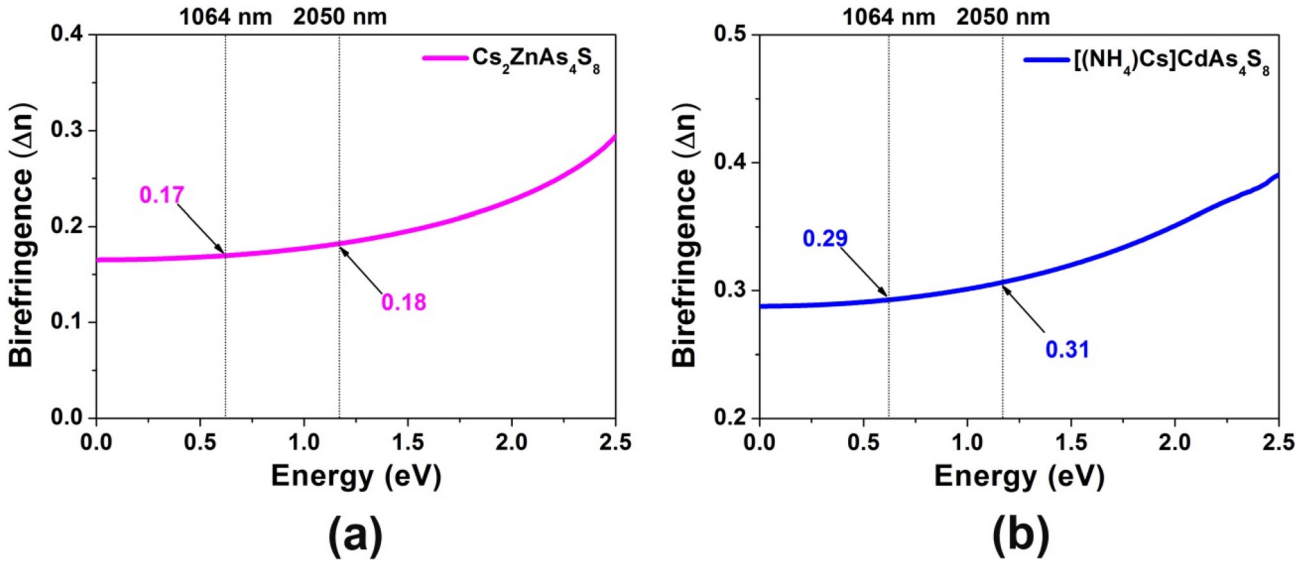

Fig. 5 Curves of the calculated birefringence (Δn) as a function of energy (eV) for (a) $Cs_2ZnAs_4S_8$ and (b) $[(NH_4)Cs]CdAs_4S_8$.

Conclusions

In conclusion, two new members of the multinary X-TM-As-S family, $Cs_2ZnAs_4S_8$ and $[(NH_4)Cs]CdAs_4S_8$, have been prepared by a simple surfactant–thermal method. Although they have similar chemical stoichiometry 2–1–4–8, they undergo an intriguing dimensional transition from a 3D framework to a 2D layered structure. The optical absorption spectra and photoelectric results confirm that both the thioarsenates are wide-bandgap semiconductors and $Cs_2ZnAs_4S_8$ exhibits a better photocurrent response than $[(NH_4)Cs]CdAs_4S_8$ under the same test conditions. Meanwhile they also show large birefringence. In particular for $[(NH_4)Cs]CdAs_4S_8$, the calculated birefringence values are 0.29@1064 nm and 0.31@2050 nm, respectively, suggesting its potential for application as a dual-waveband birefringent crystal. The analysis results of the structure–activity relationship show that the low dimensional structure of this family will be favorable for the generation of large optical anisotropy, that is, to obtain high birefringence. These results provide new insights into the exploration of novel functional chalcogenides and further research on the other physical properties of the title compounds is ongoing.

Author contributions

C. Zhang prepared the samples, and designed and carried out the experiments. S. H. Zhou carried out the theoretical calculations. Y. Xiao measured the optical properties. H. Lin and Y. Liu conceived the experiments, analyzed the results and wrote and edited the manuscript. All the authors have approved the final version of the manuscript.

Conflicts of interest

There are no conflicts to declare.

Acknowledgements

This work was supported by the National Natural Science Foundation of China (No. 52171277, 22175175 and 21771179), the Natural Science Foundation of Fujian Province (No. 2019J01133), the Fujian Science & Technology Innovation Laboratory for Optoelectronic Information of China (2021ZR118) and the Shanxi-Zheda Institute of Advanced Materials and Chemical Engineering (2022SZ-TD006).

References

1 T. K. Bera, J. I. Jang, J. B. Ketterson and M. G. Kanatzidis, Strong Second Harmonic Generation from the Tantalum Thioarsenates $A_3Ta_2AsS_{11}$ (A = K and Rb), *J. Am. Chem. Soc.*, 2009, **131**, 75–77.
2 C. D. Malliakas, D. Y. Chung, H. Claus and M. G. Kanatzidis, Superconductivity in the Narrow-Gap Semiconductor $CsBi_4Te_6$, *J. Am. Chem. Soc.*, 2013, **135**, 14540–14543.
3 L. L. Long, A. Y. Zhang, Y. X. Huang, X. Zhang and H. Q. Yu, A robust cocatalyst Pd_4S uniformly anchored onto Bi_2S_3 nanorods for enhanced visible light photocatalysis, *J. Mater. Chem. A*, 2015, **3**, 4301–4306.
4 C. D. Malliakas, D. Y. Chung, H. Claus and M. G. Kanatzidis, Superconductivity in the Narrow Gap Semiconductor $RbBi_{11/3}Te_6$, *J. Am. Chem. Soc.*, 2016, **138**, 14694–14698.

5 G. J. Tan, L. D. Zhao and M. G. Kanatzidis, Rationally Designing High-Performance Bulk Thermoelectric Materials, *Chem. Rev.*, 2016, **116**, 12123–12149.
6 N. Markus, F. Felix, K. Marcus and O. Oliver, Single crystal structure elucidation and thermoelectric properties of a long-periodically ordered germanium arsenic telluride, *J. Alloys Compd.*, 2017, **694**, 1160–1164.
7 H. Lin, Y. Y. Li, M. Y. Li, Z. J. Ma, L. M. Wu, X. T. Wu and Q. L. Zhu, Centric-to-acentric structure transformation induced by a stereochemically active lone pair: a new insight for design of IR nonlinear optical materials, *J. Mater. Chem. C*, 2019, **7**, 4638–4643.
8 P. Levinsky, C. Candolfi, A. Dauscher, J. Tobola, J. Hejtmánek and B. Lenoir, Thermoelectric properties of the tetrahedrite–tennantite solid solutions $Cu_{12}Sb_{4-x}As_xS_{13}$ and $Cu_{10}Co_2Sb_{4-y}As_yS_{13}$ ($0 \leq x, y \leq 4$), *Phys. Chem. Chem. Phys.*, 2019, **21**, 4547–4555.
9 C. Liu, Y. Xiao, H. Wang, W. X. Chai, X. F. Liu, D. M. Yan, H. Lin and Y. Liu, One-Dimensional Chains in Pentanary Chalcogenides $A_2Ba_3Cu_2Sb_2S_{10}$ (A = K, Rb, Cs) Displaying a Photocurrent Response, *Inorg. Chem.*, 2020, **59**, 1577–1581.
10 H. Lin, W. B. Wei, H. Chen, X. T. Wu and Q. L. Zhu, Rational design of infrared nonlinear optical chalcogenides by chemical substitution, *Coord. Chem. Rev.*, 2020, **406**, 213150.
11 M. Yan, H.-G. Xue and S.-P. Guo, Recent Achievements in Lone-Pair Cation-Based Infrared Second-Order Nonlinear Optical Materials, *Cryst. Growth Des.*, 2021, **21**, 698–720.
12 M.-M. Chen, Z. Ma, B.-X. Li, W.-B. Wei, X.-T. Wu, H. Lin and Q.-L. Zhu, $M_2As_2Q_5$ (M = Ba, Pb; Q = S, Se): a source of infrared nonlinear optical materials with excellent overall performance activated by multiple discrete arsenate anions, *J. Mater. Chem. C*, 2021, **9**, 1156–1163.
13 Y. Xiao, M. M. Chen, Y. Y. Shen, P. F. Liu, H. Lin and Y. Liu, $A_3Mn_2Sb_3S_8$ (A = K and Rb): a new type of multifunctional infrared nonlinear optical material based on unique three-dimensional open frameworks, *Inorg. Chem. Front.*, 2021, **8**, 2835–2843.
14 M.-M. Chen, S.-H. Zhou, W.-B. Wei, B.-X. Li, M.-Y. Ran, X.-T. Wu, H. Lin and Q.-L. Zhu, $RbBiP_2S_6$: A Promising IR Nonlinear Optical Material with a Giant Second-Harmonic Generation Response Designed by Aliovalent Substitution, *ACS Mater. Lett.*, 2022, **4**, 1264–1269.
15 H. Chen, M.-Y. Ran, W.-B. Wei, X.-T. Wu, H. Lin and Q.-L. Zhu, A comprehensive review on metal chalcogenides with three-dimensional frameworks for infrared nonlinear optical applications, *Coord. Chem. Rev.*, 2022, **470**, 214706.
16 H. Chen, W. B. Wei, H. Lin and X. T. Wu, Transition-metal-based chalcogenides: A rich source of infrared nonlinear optical materials, *Coord. Chem. Rev.*, 2021, **448**, 214154.
17 A. Abudurusuli, K. Wu, Y. Rouzhahong, Z. Yang and S. Pan, $Na_6Zn_3M^{III}{}_2Q_9$ (M^{III} = Ga, In; Q = S, Se): four new supertetrahedron-layered chalcogenides with unprecedented vertex-sharing T_3-clusters and desirable photoluminescence performances, *Inorg. Chem. Front.*, 2018, **5**, 1415–1422.
18 M.-M. Chen, S.-H. Zhou, W.-B. Wei, X.-T. Wu, H. Lin and Q.-L. Zhu, Phase Matchability Transformation in the Infrared Nonlinear Optical Materials with Diamond-Like Frameworks, *Adv. Opt. Mater.*, 2022, **10**, 2102123.
19 C. Li, W. Yin, P. Gong, X. Li, M. Zhou, A. Mar, Z. Lin, J. Yao, Y. Wu and C. Chen, Trigonal Planar $[HgSe_3]^{4-}$ Unit: A New Kind of Basic Functional Group in IR Nonlinear Optical Materials with Large Susceptibility and Physicochemical Stability, *J. Am. Chem. Soc.*, 2016, **138**, 6135–6138.
20 Y. D. Wu and W. Bensch, Synthesis, crystal structures, and optical properties of $NaCdPnS_3$ (Pn = As, Sb), *J. Alloys Compd.*, 2012, **511**, 35–40.
21 R. G. lyer and M. G. Kanatzidis, $[Mn_2(AsS_4)_4]^{8-}$ and $[Cd_2(AsS_4)_2(AsS_5)_2]^{8-}$: Discrete Clusters with High Negative Charge from Alkali Metal Polythioarsenate Fluxes, *Inorg. Chem.*, 2004, **43**, 3656–3662.
22 X. Y. Tian, C. X. Du, G. T. ZhaoRi, M. G. SheLe, Y. S. Bao and M. H. Baiyin, The solvothermal synthesis and characterization of quaternary arsenic chalcogenides $CsTMAsQ_3$ (TM = Hg, Cd; Q = S, Se) using Cs^+ as a structure directing agent: from 1D anionic chains to 2D anionic layers, *RSC Adv.*, 2020, **10**, 34903–34909.
23 W. W. Xiong, E. U. Athresh, Y. T. Ng, J. Ding, T. Wu and Q. C. Zhang, Growing Crystalline Chalcogenidoarsenates in Surfactants: From Zero-Dimensional Cluster to Three-Dimensional Framework, *J. Am. Chem. Soc.*, 2013, **135**, 1256–1259.
24 W. W. Xiong, P. Z. Li, T. H. Zhou, A. Y. Tok, R. Xu, Y. Zhao and Q. C. Zhang, Kinetically Controlling Phase Transformations of Crystalline Mercury Selenidostannates through Surfactant Media, *Inorg. Chem.*, 2013, **52**, 4148–4150.
25 C. Liu, Y. Y. Shen, P. P. Hou, M. J. Zhi, C. M. Zhou, W. X. Chai, J. W. Cheng and Y. Liu, Hydrazine-Hydrothermal Synthesis and Characterization of the Two New Quaternary Thioantimonates(III) $BaAgSbS_3$ and $BaAgSbS_3{\cdot}H_2O$, *Inorg. Chem.*, 2015, **54**, 8931–8936.
26 W. W. Xiong and Q. C. Zhang, Surfactants as Promising Media for the Preparation of Crystalline Inorganic Materials, *Angew. Chem., Int. Ed.*, 2015, **54**, 11616–11623.
27 Y. Y. Shen, C. Liu, P. P. Hou, M. J. Zhi, C. M. Zhou, W. X. Chai, Q. C. Zhang and Y. Liu, Facile surfactant-thermal syntheses and characterization of quaternary copper thioantimonates(III) ACu_2SbS_3 (A = K, Rb, Cs), *J. Alloys Compd.*, 2016, **660**, 171–177.
28 D. M. Yan, P. P. Hou, C. Liu, W. X. Chai, X. R. Zheng, L. D. Zhang, M. J. Zhi, C. M. Zhou and Y. Liu, Effect of alkali cations on two-dimensional networks of two new quaternary thioarsenates (III) prepared by a facile surfactant-thermal method, *J. Solid State Chem.*, 2016, **241**, 47–53.
29 D. M. Yan, C. Liu, W. X. Chai, X. R. Zheng, L. D. Zhang, M. J. Zhi, C. M. Zhou, Q. C. Zhang and Y. Liu, Facile Hydrazine-Hydrothermal Syntheses and Characterizations of Two Quaternary Thioarsenates(III): Two-Dimensional

$SrAg_4As_2S_6{\cdot}2H_2O$ and One-Dimensional $BaAgAsS_3$, *Chem. – Asian J.*, 2016, **11**, 1842–1848.

30 D. M. Yan, Y. Xiao, C. Liu, P. P. Hou, W. X. Chai, H. Hosono, H. Lin and Y. Liu, Two new members in the quaternary Cs-Ag-As-S family with different arrangements of Ag–S and As–S asymmetric building units: syntheses, structures, and theoretical studies, *Dalton Trans.*, 2020, **49**, 9743–9750.

31 R. Ye, B. W. Liu, X. M. Jiang, J. Lu, H. Y. Zeng and G. C. Guo, $AMnAs_3S_6$ (A = Cs, Rb): Phase-Matchable Infrared Nonlinear Optical Functional Motif $[As_3S_6]^{3-}$ Obtained via Surfactant–Thermal Method, *ACS Appl. Mater. Interfaces*, 2020, **12**, 53950–53956.

32 H. Lin, L. J. Zhou and L. Chen, Sulfides with Strong Nonlinear Optical Activity and Thermochromism: $ACd_4Ga_5S_{12}$ (A = K, Rb, Cs), *Chem. Mater.*, 2012, **24**, 3406–3414.

33 H. Lin, H. Chen, Y. J. Zheng, J. S. Yu, X. T. Wu and L. M. Wu, Coexistence of Strong Second Harmonic Generation Response and Wide Band Gap in $AZn_4Ga_5S_{12}$ (A = K, Rb, Cs) with 3D Diamond-like Frameworks, *Chem. – Eur. J.*, 2017, **23**, 10407–10412.

34 Y. J. Zheng, Y. F. Shi, C. B. Tian, H. Lin, L. M. Wu, X. T. Wu and Q. L. Zhu, An Unprecedented Pentanary Chalcohalide with the Mn Atoms in Two Chemical Environments: Unique Bonding Characteristics and Magnetic Properties, *Chem. Commun.*, 2019, **55**, 79–82.

35 J. Tauc, R. Grigorovici and A. Vancu, Optical Properties and Electronic Structure of Amorphous Germanium, *Phys. Status Solidi*, 1966, **15**, 627.

36 Y. Takeuchi and N. Haga, On the crystal structures of seligmannite, $PbCuAsS_3$, and related minerals, *Z. Kristallogr. - Cryst. Mater.*, 1969, **130**, 254–260.

37 H. G. Yao, M. Ji, S. H. Ji and Y. L. An, Synthesis, structure and characterization of two new copper(I)-thioarsenates (III) constructed by the $[AsS_3]^{3-}$ and CuS_x units, *J. Solid State Chem.*, 2013, **198**, 289–294.

38 C. Liu, P. P. Hou, W. X. Chai, J. W. Tian, X. R. Zheng, Y. Y. Shen, M. J. Zhi, C. M. Zhou and Y. Liu, Hydrazine-hydrothermal syntheses, characterizations and photoelectrochemical properties of two quaternary chalcogenidoantimonates (III) $BaCuSbQ_3$ (Q = S, Se), *J. Alloys Compd.*, 2016, **679**, 420–425.

39 C. Li, Z. Lin, L. Kang, Z. Lin, H. Huang, J. Yao and Y. Wu, Sn_2SiS_4, synthesis, structure, optical and electronic properties, *Opt. Mater.*, 2015, **47**, 379–385.

40 L. N. Nie and Q. C. Zhang, Recent progress in crystalline metal chalcogenides as efficient photocatalysts for organic pollutant degradation, *Inorg. Chem. Front.*, 2017, **4**, 1953–1962.

41 L. N. Nie, G. F. Liu, J. Xie, T. T. Lim, G. S. Armatas, R. Xu and Q. C. Zhang, Syntheses, crystal structures, and photocatalytic properties of two ammonium-directed Ag-Sb-S complexes, *Inorg. Chem. Front.*, 2017, **4**, 954–959.

42 M.-Y. Ran, S.-H. Zhou, W.-B. Wei, B.-J. Song, Y.-F. Shi, X.-T. Wu, H. Lin and Q.-L. Zhu, Quaternary Chalcohalides $CdSnSX_2$ (X = Cl or Br) with Neutral Layers: Syntheses, Structures, and Photocatalytic Properties, *Inorg. Chem.*, 2021, **60**, 3431–3438.

43 M.-Y. Li, X.-Y. Xie, X.-T. Wu, X.-F. Li and H. Lin, Quaternary Selenophosphate $Cs_2ZnP_2Se_6$ Featuring Unique One-dimensional Chains and Exhibiting Remarkable Photoelectrochemical Response, *Chin. J. Struct. Chem.*, 2021, **40**, 246–255.

44 K. Burke, Perspective on density functional theory, *J. Chem. Phys.*, 2012, **136**, 150901.

45 M. Y. Ran, Z. J. Ma, H. Chen, B. X. Li, X. T. Wu, H. Lin and Q. L. Zhu, Partial Isovalent Anion Substitution to Access Remarkable Second-Harmonic Generation Response: A Generic and Effective Strategy for Design of Infrared Nonlinear Optical Materials, *Chem. Mater.*, 2020, **32**, 5890–5896.

46 M.-Y. Ran, Z. Ma, X.-T. Wu, H. Lin and Q.-L. Zhu, $Ba_2Ge_2Te_5$: a ternary NLO-active telluride with unusual one-dimensional helical chains and giant second-harmonic-generation tensors, *Inorg. Chem. Front.*, 2021, **8**, 4838–4845.

47 C. Liu, S.-H. Zhou, C. Zhang, Y.-Y. Shen, X.-Y. Liu, H. Lin and Y. Liu, $CsCu_3SbS_4$: rational design of a two-dimensional layered material with giant birefringence derived from Cu_3SbS_4, *Inorg. Chem. Front.*, 2022, **9**, 478–484.

48 M.-Y. Ran, S.-H. Zhou, B.-X. Li, W.-B. Wei, X.-T. Wu, H. Lin and Q.-L. Zhu, Enhanced Second-Harmonic-Generation Efficiency and Birefringence in Melillite Oxychalcogenides $Sr_2MGe_2OS_6$ (M = Mn, Zn, and Cd), *Chem. Mater.*, 2022, **34**, 3853–3861.

49 H.-D. Yang, M.-Y. Ran, S.-H. Zhou, X.-T. Wu, H. Lin and Q.-L. Zhu, Rational Design via Dual-Site Aliovalent Substitution Leads to an Outstanding IR Nonlinear Optical Material with Well-Balanced Comprehensive Properties, *Chem. Sci.*, 2022, **13**, 10725–10733.

50 Y.-F. Shi, Z. Ma, B.-X. Li, X.-T. Wu, H. Lin and Q.-L. Zhu, Phase matching achieved by isomorphous substitution in IR nonlinear optical material $Ba_2SnSSi_2O_7$ with an undiscovered $[SnO_4S]$ functional motif, *Mater. Chem. Front.*, 2022, DOI: **10.1039/D2QM00621A**.